Proceedings of ASME Turbo Expo 2011
GT2011
June 6-10, 2011, Vancouver, British Columbia, Canada

GT2011-45192

INVESTIGATION OF EFFECT OF END WALL CONTOURING METHODS ON A TRANSONIC TURBINE BLADE PASSAGE

Kapil Panchal, Santosh Abraham, Srinath V Ekkad, Wing Ng
Department of Mechanical Engineering, Virginia Tech
Blacksburg, Virginia, USA

Barry J Brown
Florida Turbine Technologies, Inc.
Jupiter, Fl, USA

Anthony Malandra
Siemens Power Generation
Orlando, Fl, USA

ABSTRACT

End wall contouring has been widely studied during past two decades for secondary loss reduction in turbine passages. Recent non-axisymmetric end wall contouring methods have shown more promise for loss reduction as compared to the axisymmetric end wall contouring methods used in initial studies. The end wall contouring methods have shown definite promise, especially, for the turbine passages at low design exit Mach numbers. A class of methods exists in the literature where the end wall surface is defined by using a combination of two curves. These curves specify surface topology variation in streamwise and pitchwise directions. Another class of methods depends on surface contour optimization, in which the modification of surface contours is achieved by changing the control point locations that define the surface topology. A definitive, passage design parameter based method of contouring is still not available. However, a general guideline for the trend of contour variation, along pitchwise and streamwise direction, can certainly be extrapolated from the existing literature. It is not clear, however, whether such a trend can be fitted to any blade profile to achieve, least of all a non-optimum but a definite, reduction in losses. Moreover, almost all of the existing studies have focused on end wall contouring of passages with low exit Mach numbers. Some researchers, indeed, have used blades designed for high turning and high exit Mach number. However, such studies were done at Mach number well below the intended design condition. A study of effect of end wall contouring on a high turning blade with high design exit Mach number is not available in open literature.

The present study investigates the effect of application of three different types of end wall contouring methods through numerical simulation, on a high turning transonic turbine blade passage. The main contouring method is based on total loss reduction criterion which is described here in detail. The contouring methodology described here avoids the deficiency of current commercial mesh generation software in context of automated meshing and provides a robust end wall optimization methodology. The geometry that gives minimum SKE values is compared with this loss optimized geometry. Additionally, a normalized contoured surface topology was extracted from a previous study that has similar blade design parameters and this surface was fitted to the turbine passage under study in order to investigate the effect of such trend based surface fitting. This contour geometry has also been compared with the other two contour geometries. Aerodynamic response of these geometries has been compared in detail with the baseline case without any end wall contouring. A comparison of shape and location of end wall contours on aerodynamic performance has been provided. The results indicate that end wall contouring for transonic turbine blades may not result in as significant gains at design conditions as those claimed for low speed turbine passages in previous studies.

INTRODUCTION

Onset of horseshoe vortex and development of secondary flow in turbine passages has been studied by many researchers. Controlling secondary flow within a turbine passage has been an area of active research for some time. Turbine passage end wall contouring is one out of many methods available for passage flow control. Many methods of end wall contouring have been proposed.

During one of the earliest studies, Morris et al [1] studied the effect of meridional end wall contouring and demonstrated a reduction in overall secondary loss by 25%. The nonaxisymmetric end wall profile used in the study, however, did not show any promising results. The study was conducted at a very low Mach number and Reynolds number as compared to those encountered in modern HP turbines.

Kopper et al [2] studied an axisymmetrically contoured vane passage at high exit Mach number of 0.85 and noted about 17% reduction in mass averaged total losses. The vane was a low turning angle (70^o) profile with a low aspect ratio of about 0.5. Mass contained in the secondary flow structures is a significant portion of the total mass flow in such cases. The secondary losses were over half of the total losses. The experiments conducted by Duden et al [3] with a different type of meridional end wall profiling, for a highly loaded turbine cascade with about 100^o turning, however, did not show any significant overall reduction in overall losses.

Many other researchers tried such axisymmetric end wall contouring (EWC), especially during 1990s, but none of the studies showed significant and definite improvement for high exit Mach number blades.

Rose [4] proposed a method of nonaxisymmetric end wall contouring using a combination of two profiles in which these profiles specified axial and circumferential shape variations for the end wall of an HP turbine NGV. He suggested a sinusoidal circumferential profile variation for subsonic flow field and a Fourier series based profile variation for supersonic flow field.

Harvey et al [5-6] used a combination of Fourier series perturbations in pitchwise direction and a b-spline curve fitted in axial direction in order to generate nonaxisymmetric end wall profile for a 100^o turning turbine blade cascade. Experimental analysis carried out at a very low Mach number (~0.1) showed reduction in total loss by about 20%. CFD predictions used for the design iterations had reported a total loss reduction of only about 0.5%. This method has been used in many other cascade studies as well as real engine experiments and has been found to produce improved results for similar low exit Mach number applications.

Hartland [7] reported 6% reduction in secondary losses for and end wall surface that was defined using a half cosine wave in pitchwise direction and an axial profile based on the blade camber line shape. The investigations were done on the sameDurham cascade used by Harvey et al [6].

Nagel et al [8] used combination of pressure and suction side shape functions with a circumferentially varying decay function to generate end wall profile for a turbine vane cascade. These functions were based on the passage design parameters. The exit Mach number for the flow was reported to be 0.59.

Saha et al [9] followed the approach of generating a geometry using combination of streamwise and pitchwise height variation curves. They numerically studied nine geometries with such nonaxisymmetric contours. Reported reduction in mass averaged total losses was about 3.2% through numerical computations for the finally selected geometry. During the low Mach number experimental investigations for this blade profile, Gustafson et al [10] reported 50% reduction in mass averaged pressure losses.

Prainser et al [11] used direct surface modification using control point heights to generate profiled end wall. Numerical computations showed 12% reduction in total row-loss for the optimized end wall. However, the experimental results showed 25% reduction for the same geometry. The exit Mach number was about 0.1, a very low value.

Few important observations can be made from this information. Firstly, most of these studies were done at low exit Mach numbers and for moderate turning airfoils. The only study that was performed at very high Mach number was done on an axisymmetrically profiled end wall of a vane. There has been no published computational or experimental study done on a high turning transonic blade at a high exit Mach numbers.

For the studies where numerical computations were used [5-6,9-11], CFD results often under predicted the magnitude of loss as well as the change in loss as compared to the experimental results. However, CFD results indeed captured correct trends and the optimized geometries indeed showed improved performance.

A large variety of end wall contouring methods exists in literature. However, they broadly fall into either curve combination based method or direct surface modification method. These studies indicate that it is possible to have a general guideline regarding the end wall shape variation along the flow passage. For example, Snedden et al [12] applied Durham cascade [5-6] hub profile to the annular end wall of a 1½ stage rotating rig and observed about 0.4% improvement in rotor efficiency. However, the rotor exit relative velocities were very low in the range of about 50 m/s. The sensitivity of change in loss values by fitting end wall contours designed for a high exit Mach number turbine passage to another turbine passage with similar design parameters has, however, not been studied.

This study numerically investigates the effect of end wall contouring methods on a transonic blade passage. The blade profile used for the study represents a high turning (~127^o), high exit Mach number (M_{iso}~0.87) profile of the first stage of an HP turbine blade. The blade passage exit aspect ratio is 1.45.

The immediately following sections describe the details of passage geometry generation, end wall geometry generation and corresponding mesh generation methods. Details of mesh refinement study, blade loading validation and mesh noise assessment have also been provided in the relevant sections.

The present study also provides details of optimization methodology used for the end wall contouring of the transonic turbine blade profile. Two geometries, one with minimum total loss values and one with minimum SKE values, have been compared for their aerodynamic performance. In addition to that, the contouring method used by Saha et al [9] and Gustafson et al [10] has been normalized, scaled and applied to the passage under study. Both, the optimized and surface fitted, end walls were compared to decide whether it is possible to achieve, even a non-optimum but certain, loss reduction by fitting an end wall contour shape of one blade passage to another blade passage with similar design parameters.

NOMENCLATURE

C_{ax}	Axial chord length
M_{iso}	Isentropic Mach number
	$M_{iso} = \sqrt{\left(\left(\frac{p_{0in}}{p_s}\right)^{\frac{\gamma-1}{\gamma}} - 1\right)\frac{2}{\gamma-1}}$
p_{0in}	Pitchwise average stagnation pressure at inlet midspan
p_0	Local stagnation pressure
p_s	Local static pressure
p_{sexit}	Pitchwise average static pressure on angled end wall 0.5 C_{ax} downstream of the trailing edge
SKE	Secondary kinetic energy $\frac{\rho(v_{sec}^2+w_{sec}^2)}{2}$
v_{sec}	Secondary velocity component in blade-to-blade direction measured on a plane perpendicular to the exit flow direction
w_{sec}	Secondary velocity component in spanwise direction measured on a plane perpendicular to the exit flow direction

Greek Letters

ω	Loss coefficient $\frac{p_{0in}-p_0}{p_{0in}-p_{sexit}}$

PASSAGE GEOMETRY GENERATION

A Matlab^{TM} routine, developed in-house, was used to generate the required passage curves for 3D CFD analysis. Initially the curves for the 2D turbine passage (Fig. 1) are generated, which are then used to generate a 3D passage. The parameters for the b-spline curves for the periodic sides of the passage (Fig. 1) can be selected and manipulated using the Matlab^{TM} routine. In order to closely simulate the blade loading which is similar to that on the actual blade, the exit span is increased relative to the inlet span. This results in one end wall diverging from inlet to exit at an angle of 13^o. Hence, the passage represents a quasi 2D linear cascade. The inlet to the turbine passage model is 0.5 axial chords upstream of the axial leading edge and the outlet is located 1.5 axial chords downstream of the trailing edge.

END WALL GEOMETRY GENERATION

Two different types of end wall geometries have been studied. However, the overall procedure for end wall surface generation for the simulation remains the same. A Matlab^{TM} routine has been developed in-house that facilitates interactive placement of control points within the passage as shown in Fig. 2. It is possible to place a set of control points at any axial location. Also, at a given axial location, any number of control points can be placed which are then used to generate a b-spline curve in pitchwise direction. The contoured surface passes through these control points. The axial direction represents the direction of engine axis.

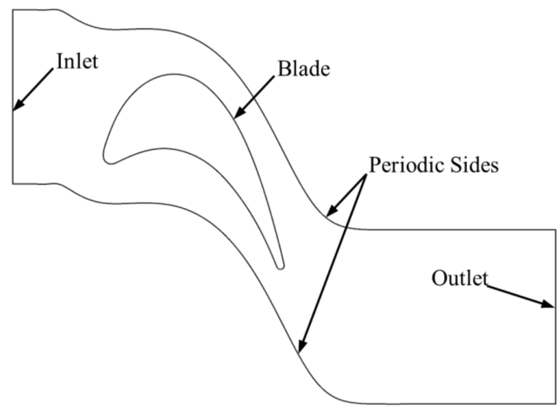

FIGURE 1 : 2D PASSAGE GEOMETRY

At a given axial location, the set of control points has a certain number of independent control points as shown in Fig 2. Height, in the direction perpendicular to the page, of these control points can be changed independently. The heights of dependent control points are calculated in such a way that surface continuity is maintained in pitchwise direction. An example of such height adjustment is as shown in Fig. 3 for a set of control points.

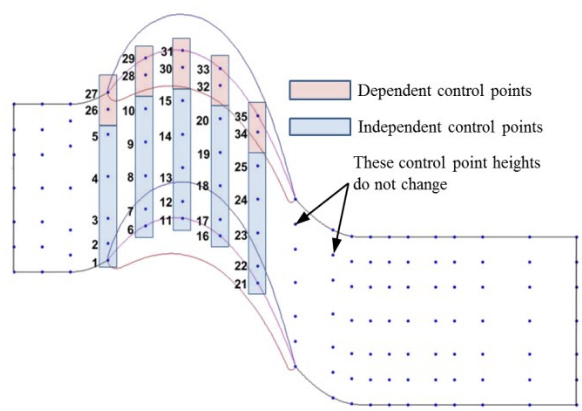

FIGURE 2 : CONTOURED SURFACE CONTROL POINT PLACEMENT

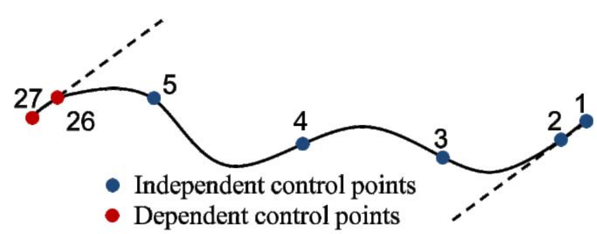

FIGURE 3 : B-SPLINE CURVE FITTING AT AN AXIAL LOCATION

A set of parameter values for each independently controllable point, as a fraction of maximum height variation, is specified during design iterations. The maximum height variation, i.e. maximum peak or trough height in comparison to the non-contoured end wall, for this study was specified to be about $\pm 5\%$ of inlet span. The Matlab^{TM} routine decides the control point heights based on these parameter values. A b-spline curve is fitted to pass through these control points. The algorithm to fit such a b-spline was adopted from Ref. [13]. The heights of dependent control points are calculated in such a way that the b-spline maintains C^0 continuity and an approximate C^1 continuity in pitchwise direction. Heights of curve end points are restricted to be the same, for example points 1 and 27 in Fig. 3, to maintain C^0 continuity. Second point from each end of the curve is used to maintain an approximate C^1 continuity. For example, height of the dependent control point 26 is set in such a way that the slop of line passing through points 27 and 26 is numerically close to the slope of line passing through points 1 and 2 as shown in Fig. 3. Once the equation of b-spline at a given axial location is available, such a b-spline is extended multiple times in pitchwise direction on both the sides to ensure surface continuity during surface generation process. It may be noted that such continuity is required only in upstream and downstream regions. The control points span from one camber line to another camber line within the passage, as shown in Fig. 2, and therefore, such continuity is not a requirement within the passage.

Once the curve points are available at each axial location, a surface is lofted through all the curves, which is the required contoured surface for specified parameter values. It is possible to have a very high flexibility in surface generation as any number of points can be specified at a given axial location. However, increased number of independent control point increases number of iterations required for the optimization process.

During the present study 25 control points within the passage were used as independent control points. This limits the extent of contouring from 1.25 axial chords upstream up to the axial trailing edge of the blade.

PASSAGE MESH GENERATION

A 2D mesh, as shown in Fig. 4, is initially generated using ICEM CFD commercial mesh generation software.

This mesh is then used as input to a Matlab^{TM} routine that generates 3D baseline mesh with non-contoured angled end wall as shown in Fig. 5. The mesh generated by the routine is a very high quality mesh with minimum mesh quality of 0.5 and a highly orthogonal mesh with about 92% of cells with minimum angle of 63^o. Minimum angle for the whole domain was found to be 27^o. The final mesh used after mesh refinement study showed y^+ values below or close to 1 for most of the region with the highest y^+ values close to 2 in a very small region near trailing edge.

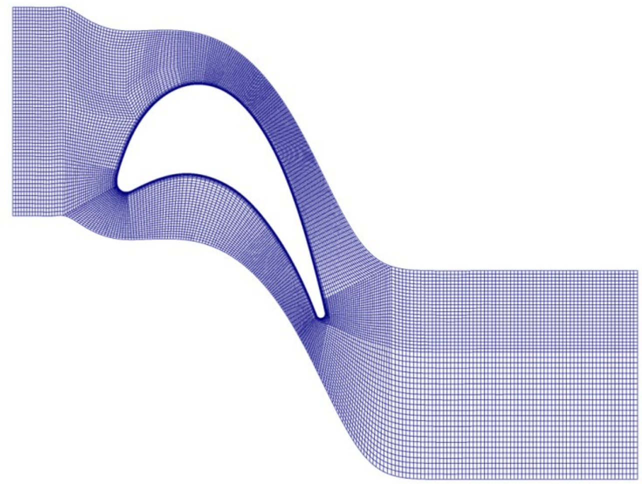

FIGURE 4 : INITIAL 2D MESH

MESH MODIFICATION FOR END WALL CONTOURS

Most commercially available grid generation software programs have surface modeling based geometry generation. This creates problems related to surface stitching where two surfaces meet at an angle, especially when mesh generation is automated. In addition, negative volume problems are generally encountered when mesh needs to be projected on to a highly distorted contoured surfaces like those used in the present study.

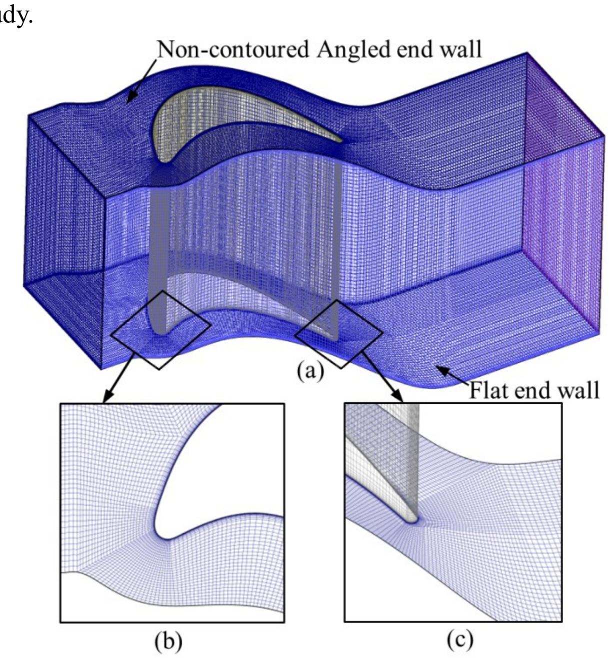

FIGURE 5 : (A) 3D BASELINE MESH WITH ONE ANGLED END WALL (B) ENLARGED REGION NEAR LEADING EDGE (C) ENLARGED REGION NEAR TRAILING EDGE

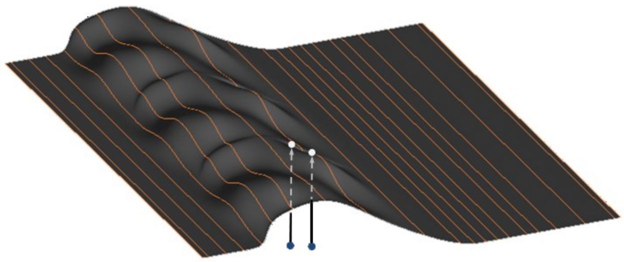

FIGURE 6 : NODE PROJECTION BASED MESH MODIFICATION

A Matlab™ routine was developed, that avoids such mesh generation problems. The b-spline curves are used to generate a lofted contoured surface as mentioned before. An example of the pitchwise extended contoured end wall surface is shown in Fig. 6.

It may be noted that the contouring was done on the angled end wall. The distance between mesh nodes on flat end wall and corresponding mesh nodes on the contoured end wall is calculated by projecting the non-contoured angled end wall nodes on the contoured end wall. All the mesh points are then shifted in spanwise direction using the MATLAB™ routine in order to accommodate the change in heights at different locations. It was observed that the mesh used for this study is sufficiently dense and hence there was not much mesh distortion due to such node movement.

Such a node projection based approach facilitates very robust automated mesh generation capability which is essential for optimization runs. The routine is able to successfully generate good mesh even for highly contoured geometries.

CFD MODEL AND BOUNDARY CONDITIONS

Various boundary conditions applied on the model are shown in Fig. 1. Inlet total pressure profile was experimentally measured and applied as inlet boundary condition. Uniform total temperature conditions were specified at the inlet. Due to the very high turning angle of the blades, the flow starts turning even before the leading edge and an induced incidence angle is observed just before the leading edge. Hence, a slightly positive incidence angle was specified at the inlet in order to get design incidence angle near the blade leading edge. Once the simulation results were available, many contoured geometries were checked to confirm that the flow close to the blade leading edge closely matches the design inlet angle. This ensures correct design angle during the optimization study. Medium turbulence intensity of 5%, that closely matches the turbulence level observed during the experimental study done on this blade passage, was specified at the inlet boundary.

Prescribed average static pressure condition was specified at the outlet boundaries. Translational periodic boundary conditions were prescribed at the periodic sides. End walls and blade surface were prescribed adiabatic wall boundary condition with zero slip velocity.

SST $k-\omega$ turbulence model was used based on past experience. Convergence criteria form RMS residuals was chosen to be 5×10^{-5} based on the mesh refinement study. The CFD solver produced airfoil loading results, that are in reasonably good agreement with the experimental results as shown in Fig. 7 and hence the code is considered validated.

Fully 3D, viscous CFD solver CFX version 12.1 was used for the simulations performed in this study.

The CFD solver offers three different options for the advection terms: (1) 1st order upwind scheme (2) 2nd order high resolution scheme and (3) a blend factor scheme combining both the upwind and the high resolution scheme. Blend factor value of 0 refers to the purely upwind scheme whereas the value 1 refers to the purely high resolution scheme. Hence, a value between 0 and 1 can be used as a calibration factor to achieve better agreement of CFD results with the experimental values. As mentioned in the following section, the loss coefficient predictions obtained with high resolution scheme showed lower values of loss coefficients as compared to the experimental values. The effect of inlet boundary layer profile, turbulence model and advection scheme were studied. The change in inlet boundary layer profile or turbulence model did not show any significant improvement as compared to the experimental results. However, a good agreement could be obtained by using blend factor scheme with a proper blend factor value. Loss profiles created using pitch averaged values at different spans were used for comparison between CFD and experimental results. The comparisons were made at two locations, planes (3) and (4), as shown in Fig. 13. It was found that the difference between the mass averaged loss coefficient at plane (3) (which is also the optimization objective) for the high resolution scheme and the blend factor scheme remained almost constant. Moreover, the high resolution scheme, although under-predicted the losses by an almost constant value, provided better agreement with the experimentally observed shapes of loss structures at plane (4). Hence, the high resolution scheme was used for this study. It may be noted that the difference in loss coefficient value between the high resolution scheme and the blend factor scheme remains constant hence the optimization algorithm will result in almost the same geometry even if the blend factor scheme were used.

MESH REFINEMENT STUDY AND VALIDATION

Three grids with a uniform mesh refinement factor of 1.5 were used for the mesh refinement study on the baseline (non-contoured) geometry. The number of nodes in baseline mesh is about 1.5^3 times more than coarse mesh as the refinement is uniform in each direction. Similarly, the number of nodes in fine mesh is about 1.5^3 times more than those in baseline mesh as shown in Table 1. The mesh uses near wall grid bunching close to the blade and the end walls to simulate boundary layer flow more accurately. This bunching was selected in such a way that y^+ values remain below 1 for fine and baseline mesh and close to 1 for coarse mesh for most of the domain cells.

The objective of the optimization study was to minimize the total pressure loss 1.0 axial chord downstream of the axial trailing edge. Hence, this loss coefficient was chosen as the performance parameter for the refinement study. CFD simulations were performed for all the meshes with identical boundary conditions. Richardson extrapolation method [14] was used to calculate the observed order of accuracy of the scheme. Simulation results were obtained with very stringent convergence criteria for RSM residuals, e.g. 1×10^{-12} for the baseline mesh, and were used in the Richardson extrapolation formula as the exact solution of discretized equations. The observed order of accuracy for the CFD scheme used was found to be 1.37. The magnitude of discretization error in the value of the loss coefficient at design condition was found to be about 6.5% of the loss coefficient value, based on this observed order of accuracy. Although the basic scheme is second order accurate, the overall formal order of accuracy of the CFD solver used is not known. Hence, it was not possible to calculate Roche's grid convergence index [14]. However, for most commercial second order schemes, the formal order of accuracy is well below second order and therefore the discretization error estimate of 6.5% is considered sufficiently accurate.

TABLE 1 : MESH SIZES USED FOR REFINEMENT STUDY

Mesh	Number of nodes
Coarse	591468
Baseline	1812030
Fine	6559938

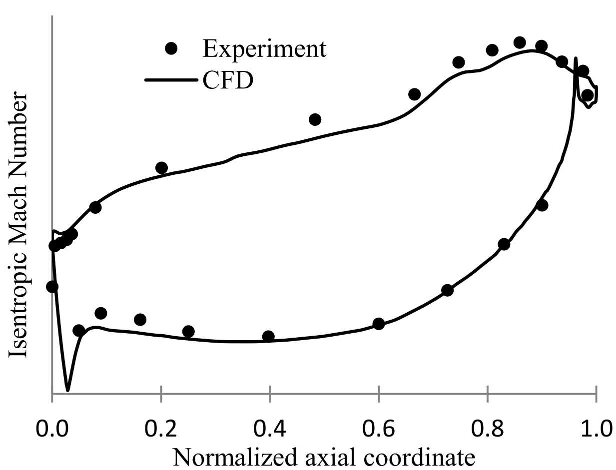

FIGURE 7 : EXPERIMENTAL AND CFD RESULTS FOR BLADE LOADING AT DESIGN CONDITIONS

The blade loading for the baseline case without end wall contouring at design conditions was compared with the experimental results. The results agree reasonably well as shown in Fig. 7.

It was observed, however, that the wake mixing after the trailing edge is not as rapid in CFD as compared to that observed in the experiments. Additionally, it was observed that the CFD results under-predict the loss coefficient values. However, many researchers mentioned in the introduction section have stated the same observation. It seems that the optimized end walls, however, do show improved results during the experimental studies in terms of loss coefficient or secondary kinetic energy. Comparison of the experimental and numerical results showed that the CFD results, indeed, predicated the correct trend of loss coefficient values as observed in experimental results at various Mach numbers and incidence angles. Hence, such CFD simulations are considered to predict correct qualitative trends.

MESH NOISE ASSESSMENT

The optimization procedure mentioned in ensuing text evaluated hundreds of contour geometries. It was essential to confirm that, for the small change in parameter values, the mesh does not give noisy (read zigzag) results due to mesh distortion. This is established by taking a vector of all the parameters and varying the parameter values with a constant relative step size within the range of each such parameter. Some arbitrarily chosen parameters are varied from maximum to minimum values whereas the others are varied from minimum to maximum. The step size is decreased until the mesh no longer produces a smooth variation in performance parameter. This sets the limit of minimum step size for the gradient based optimization method used in this study.

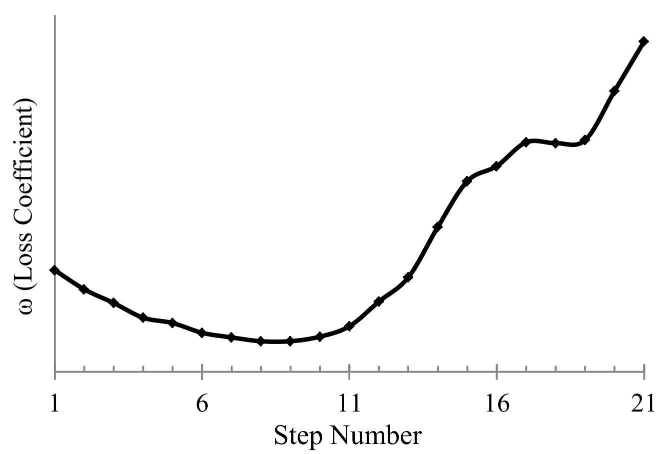

FIGURE 8 : MESH NOISE ASSESSMENT

The results of the noise assessment are as shown in Fig. 8. It can be seen that the variation is smooth until step number 15. However, the contour geometries beyond step 15 were found to be very aggressive and showed very high loss coefficient values. Hence, it can be considered that the mesh under study is sufficiently dense to give smooth monotonous variation of loss coefficient when the changes in parameter values are sufficiently small and the optimization objective is total loss minimization. The final step size chosen was 0.05 based on the results of noise assessment study.

END WALL CONTOURING OPTIMIZATION

A commercial optimization package was used for this optimization study. Sequential quadratic programming (SQP) [15] gradient based optimization technique was used. The optimization loop is shown in Fig. 9. The gradient step size used was 0.05 as mentioned in the mesh noise assessment study. The optimization objective was to minimize total loss coefficient 1.0 axial chord downstream of the trailing edge. Range of variation for each parameter was specified as a constraint condition. Additionally, a constraint was specified to restrict the maximum variation in passage mass flow rate by $\pm 1\%$ of the baseline geometry mass flow rate. An optimized geometry was achieved after about 350 contour geometry evaluations. The mesh generation program worked reliably. No failed runs were encountered during optimization process. Characteristics of optimized geometry are discussed in the "Results and discussion" section, where this optimized geometry is referred to as "Geometry A".

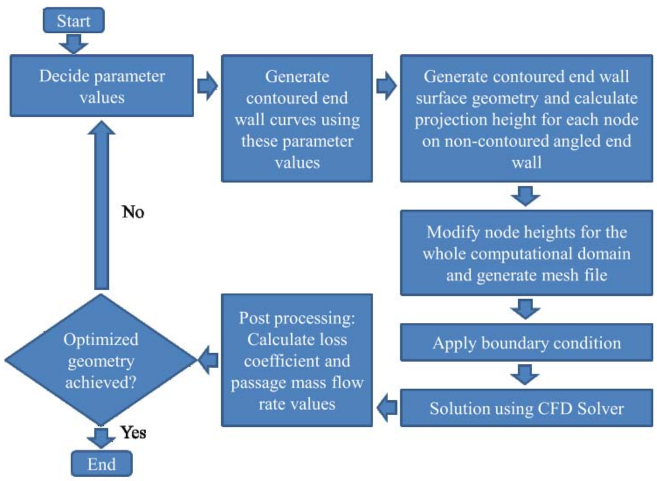

FIGURE 9 : OPTIMIZATION ALGORITHM

SKE MINIMUM GEOMETRY

Out of all the geometries evaluated, it was found that the geometry that gives minimum total loss and the geometry that gives minimum secondary kinetic energy value 1.0 axial chord downstream of the trailing edge are different. Hence, the geometry that gives minimum SKE values (Geometry B) has also been considered in this study and compared with the loss optimized Geometry A.

SHAPE FUNCTION BASED END WALL GEOMETRY

It was mentioned in the "Introduction" section that Saha et al [9] numerically tested many pitchwise and streamwise curve combination based end wall geometries and Gustafson et al [10] experimentally tested the geometry giving the best performance. The design point values and geometric dimensions for the blade used in their study are to some extent similar to the blade used in this study. Hence, the curves used for the best geometry were digitized, normalized and scaled to fit the geometry under study. Once the geometry for this end wall contours was available, a mesh file was generated using the same procedure mentioned in previous sections. Comparison of this end wall geometry (called Geometry C) to the optimized geometry (Geometry A) is discussed in the ensuing section.

RESULTS AND DISCUSSION

Geometry A (total loss optimized geometry), geometry B (geometry with minimum SKE value) and the geometry C (based on a curve combination based method from literature) all showed negligible variation in passage mass flow rate and inlet flow angle as compared to the non-contoured baseline geometry.

End wall contours for all the three geometries are as shown in Fig. 10. All the geometries show similar trend for peak and trough locations to that found in literature. There is a prominent high elevation region near pressure surface at about 0.2 C_{ax} location within the passage and a trough near the suction surface at the same location. This type of contours could not have been possible for an axisymmetrically contoured end wall and hence the importance of a non-axisymmetric contouring is evident. It may be noted that end wall contouring was restricted up to the axial trailing edge for geometries A and B. However, such restriction was not present for geometry C.

The peaks and troughs near trailing edge region are similarly prominent for all the geometries. However, such peaks occur near suction surface and troughs near pressure surface (opposite arrangement as compared to those at 0.2 C_{ax} location) for geometry A and B, whereas such peaks appear near pressure surface for geometry C and the troughs near suction surface (similar arrangement as compared to those at 0.2 C_{ax}).

Figure 11 shows variation of mass averaged total pressure loss coefficient for all the geometries including the baseline case starting from leading edge up to 1.0 C_{ax} downstream of the axial trailing edge. The values of loss coefficient are percentile fraction of the loss coefficient for the baseline case at a location 1.0 C_{ax} downstream of the trailing edge. Geometries A and B do not show much change in loss coefficient whereas geometry C shows higher loss coefficient values throughout the passage length.

It may be noted that there is marked increase in loss near trailing edge region within the passage. However, the slope of loss increase is almost the same for all the geometries. As mentioned, the prominent peak and trough locations are opposite for geometry C as compared to geometry A and geometry B in trailing edge region but the increase of loss in this region is almost the same. This indicates that for this geometry the location of peaks and troughs in the trailing edge region do not help much in reducing the losses. This also suggests that because the passage vortex height from the end wall is the highest in the trailing edge region and hence the range of maximum variation in contour height should be wider in this region in order to effectively control the secondary flow. However, there will be a limit to such maximum height variation due to the constraints on possible throat area change. This also suggests that end wall contours in the frontal region of the passage, where passage vortex mixes with corner vortex, play a significant role in loss reduction.

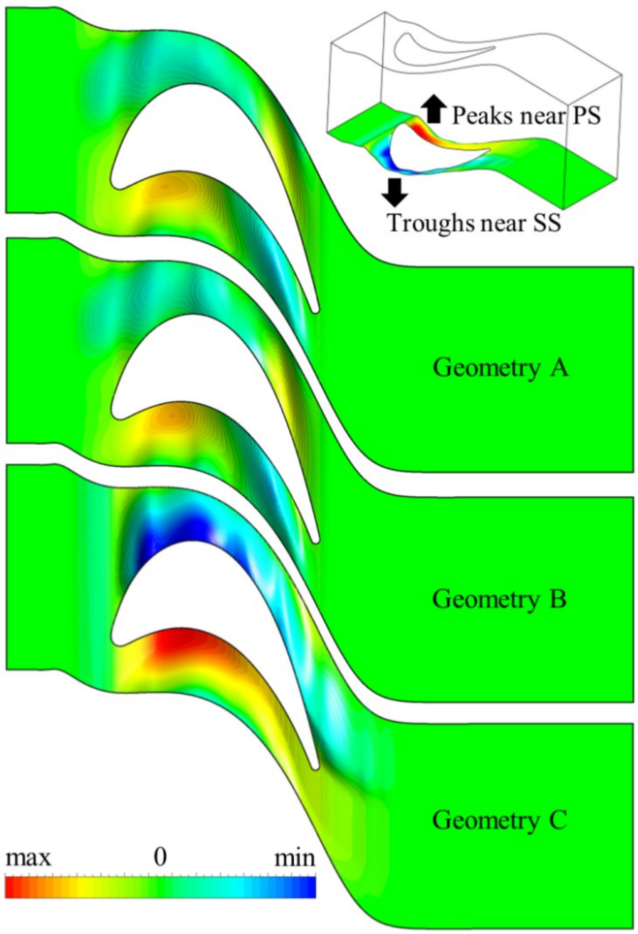

FIGURE 10 : END WALL CONTOUR HEIGHTS FOR GEOMETRIES A, B AND C

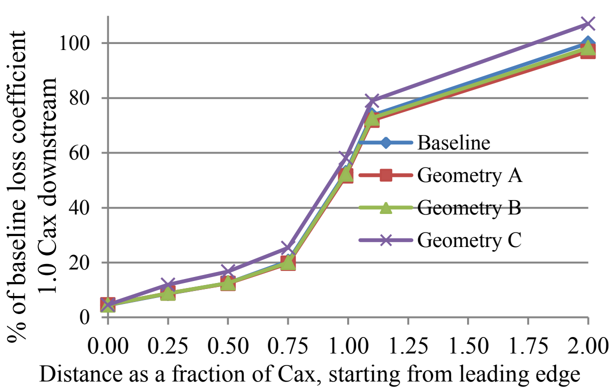

FIGURE 11 : MASS AVERAGED TOTAL PRESSURE LOSS VARIATION IN TURBINE PASSAGE

Figure 12 shows that for the loss optimized geometry A the location of maximum trough near the leading edge region closely matches the location where the passage vortex mixes with the suction side horseshoe leg. Such a mixing location is to some extent controlled by the geometry contours. As this mixing location for the non-contoured geometry is different for different airfoil profile, this suggests that even though the general trend of higher elevation from pressure side to lower elevation of contours toward suction side is maintained, the actual location and heights of the peaks and trough significantly affects the amount of loss reduction. Although it may be possible to correlate heights of contours in the mixing region as a function of blade aspect ratio and over all Mach number range by studying a large number of contoured geometries, the location of the mixing region depends not only on the overall design parameters but also on the pressure loading variation on the blade surface. Hence, it is not certain whether it is possible to reasonably predict the location of this mixing region based on the overall blade design parameters. This suggests that the optimized geometry for any blade profile should be obtained on case by case bases.

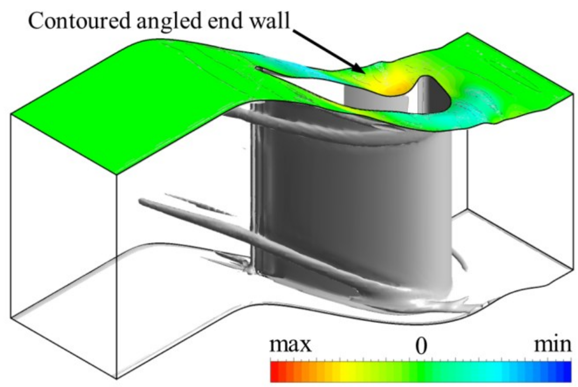

FIGURE 12 : CONTOUR HEIGHTS AND FLOW STRUCTURE WITHIN PASSAGE FOR GEOMETRY A

When compared for loss reduction performance, it was found that geometry A gives maximum reduction of about 3 % in comparison to geometry B (1.7%) in mass averaged total pressure loss at a location 1.0 C_{ax} downstream of the trailing edge. Geometry C showed an increase in loss coefficient by 7.0%. This again suggests that end wall contouring should be done on case by case bases and a general guideline may not always results in loss reduction. Table 2 shows loss performance of geometry A in comparison to the baseline geometry. The locations mentioned in the table are shown in Fig. 13.

Plots of midspan blade loading for all the geometries were found to be almost on top of that for the baseline case and hence it was expected that the profile losses may not change due to contouring which is evident from the numerical values of profile loss in Table 2. It may be noted that all the numerical values in Table 2 are shown as percentage of loss coefficient for baseline case at location (3) shown in Fig. 13.

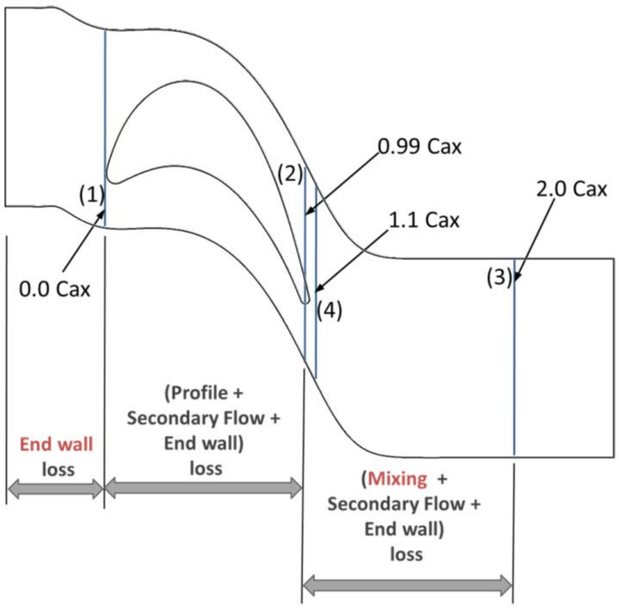

FIGURE 13 : LOCALTIONS OF LOSS MEASUREMENT

TABLE 2 : LOSS PERFORMANCE OF GEOMETRY A IN COMPARISON TO BASELINE GEOMETRY

Type of mass averaged total pressure loss and (location)	% fraction of mass averaged total pressure loss for baseline geometry at location (3)		
	Baseline (i)	Geometry A (ii)	% Change $\frac{[(ii)-(i)] \times 100}{(i)}$
$[a]$ Total loss at (2)	52.76	51.52	- 2.35
$[b]$ Profile loss at (2) *(15% of total area centered at mid-span)*	50.96	50.92	-0.08
End wall loss + secondary loss at (2) $[a-b]$	1.80	0.60	-66.67
$[c]$ Total loss at (3)	**100.00**	97.0	-3.00
Mixing loss + end wall loss + secondary loss at (3) $[c-b]$	49.04	46.08	-6.03

Profile losses for such high turning high exit Mach number blades are as much as 50% of the total losses at location (3). The secondary and end wall loss within the passage is a small amount of about 2%. Also note that even if the reduction in secondary loss is about 66%, it is in fact a very small percentage of the total loss that occurs up to location (3). Readers should note that the secondary loss was calculated from profile and total loss calculations. Particularly, profile loss is calculated using mass averaged loss value on an area (15% of total area) centered at mid-span. Such a calculation may give very high value of profile loss and may result in a considerably inaccurate value of secondary loss prediction. The authors believe that for such blades, the optimization should be based on the total loss reduction objective instead of secondary loss minimization.

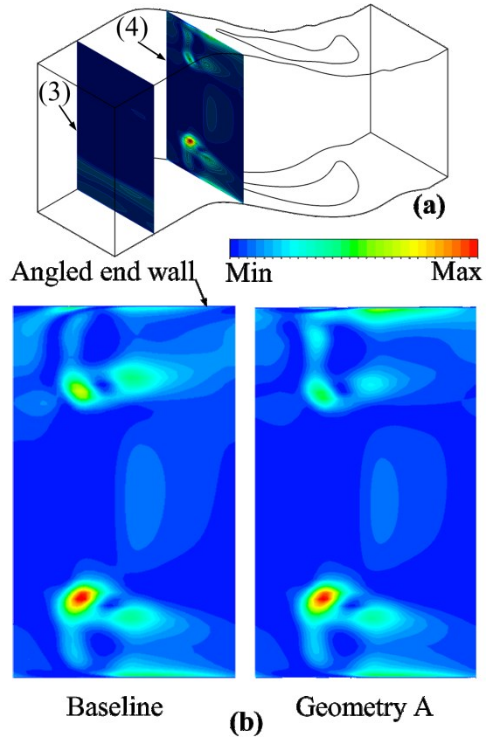

FIGURE 14 : COMPARISON OF SKE CONTOURS FOR BASELINE AND GEOMETRY A AT LOCATION (4)

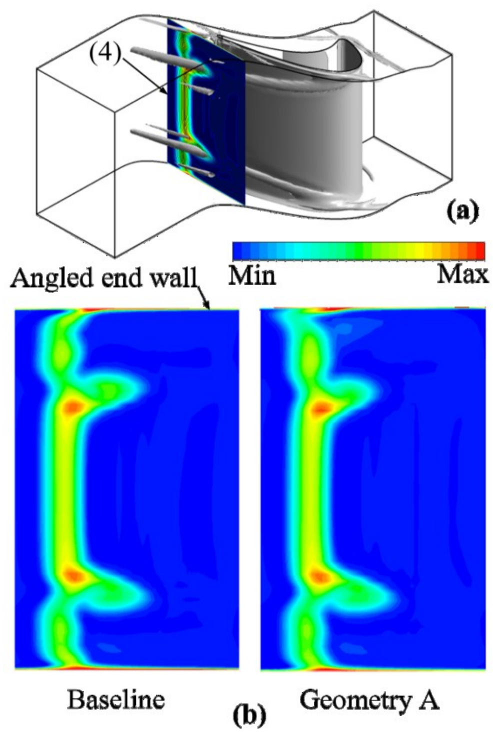

FIGURE 15 : COMPARISON OF LOSS COEFFICIENT CONTOURS FOR BASELINE AND GEOMETRY A AT LOCATION (4)

Comparison of mass averaged total loss suggests that end wall contouring results in a small percentage gain for such high turning blades subjected at high exit Mach numbers.

It may be noted that the secondary flow, end wall and mixing losses that occur after the trailing edge account for as nearly as 47%. In that case, end wall contouring in the downstream region may provide additional benefits by reducing end wall losses and wake mixing losses near the end wall by providing better flow guidance and pressure distribution. However, the authors have not evaluated the effect of downstream end wall contouring in the present study.

In addition to the effect on total pressure loss, the effect of end wall contouring on SKE and deviation angle distribution should be assessed. The mass averaged deviation angle on an area (20% of span) near the end wall for baseline and geometry A were found to be 1.63^o and 2.18^o respectively, at location 4 (Fig. 13). This is a significant difference. However, the mass flow through this area near the end wall is small as compared to the total mass flow through the whole span. Hence, the overall effect of such difference will be small. This is evident from the fact that the difference in mass averaged deviation angle values for the whole exit span at location 4 (Fig. 13) was found to be just 0.06^o, a negligibly small value.

It was found that losses and SKE are reasonably well mixed at location (3) as seen in Fig. 14(a) hence the following discussion is limited to the losses and SKE at location (4) near trailing edge. The reduction in SKE values at location (3) for geometry with minimum SKE value (geometry B) was found to be about 24% as compared to the baseline case, whereas that for the Geometry A was found to be about 22%. As the difference in reduction is not much between geometry A and geometry B, only the losses and SKE for the baseline and the loss optimized geometry A have been presented here. Figure 14(b) shows SKE contours at location (4) for the baseline geometry and geometry A. It can be seen that on the flat end wall side there is a region of very high secondary kinetic energy which is not seen on the angled end wall side. The reduction in SKE for geometry A as compared to baseline geometry is small and occurs close to the contoured end wall only. The end wall contouring for this case does not affect the flow on the opposite end wall. This is expected considering the high aspect ratio of the blade. There seems to be additional SKE production near the contoured end wall as compared to baseline due to end wall contour guided flow near trailing edge as evident from Fig. 11.

However, there is overall reduction of SKE at this location. The reduction in SKE can also be inferred from the reduced passage vortex strength as seen in Fig. 16.

Similarly, the loss contours for both the geometries as shown in Fig. 15 (b) show that the reduction in losses seems to be only near the contoured end wall in passage vortex region with a slight increase in losses near the contoured end wall. This can also be seen from reduced strength of passage vortex in the trailing edge region on contoured end wall side in Fig 16.

The region where highest loss occurs is the suction side corner vortex region as seen in Fig. 15(a) and (b). End wall contouring does not result into loss reduction in this region. Almost all of the reduction in loss seems to be due to reduction of losses in passage vortex region. In may be noted that even if the loss values are very high in corner vortex region, velocities are low and hence the mass averaged loss coefficient is affected mainly by the reduction that takes place in the passage vortex region.

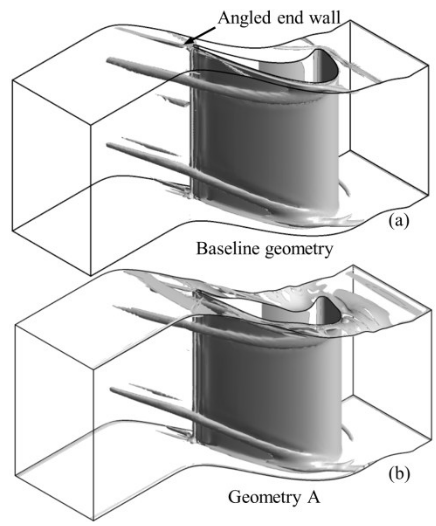

FIGURE 16 : ISOSURFACE OF SWIRLING STRENGTH FOR BASELINE AND GEOMETRY A

Comparison of SKE contours from Fig. 15 and loss contours from Fig. 16 suggests that for the baseline geometry, even if SKE values are low on the angled end wall side as compared to the flat end wall side, the loss coefficient values are almost symmetrically distributed near both the end walls. Same observation can be made for geometry A. Hence, it can be concluded that SKE is not a primary factor that affects loss production. In that case, SKE values should not be included in end wall optimization unless better flow distribution is also an objective. In fact, a total pressure loss optimized geometry will generally provide a near optimum SKE reduction.

CONCLUSIONS

An end wall contouring optimization study was carried out through numerical computations on a linear turbine cascade passage of a high turning, high exit Mach number transonic blade of the first stage of an HP turbine. The total pressure loss optimized geometry (A) was compared with the geometry that showed minimum mass averaged SKE values (geometry B). An additional geometry (C) based on the contour specifications obtained from literature was also studied.

- Although the overall contour shape agrees with that seen in the literature, the exact location and height of end wall contours are highly dependent on blade loading requiring case by case end wall contour optimization.
- Only a small reduction in mass averaged total pressure loss was observed due to end wall contouring. Profile losses for were found to be almost 98% of the total mass averaged

losses in the passage and remain unchanged even after end wall contour optimization.

- The fact that secondary losses in the passage reduced by 66% due to end wall contouring is counterbalanced by the fact that such mass averaged end wall and secondary losses are in itself a small fraction of the total loss and hence even a significant reduction in secondary losses does not impact reduction in mass averaged total loss significantly. Moreover, a small change in secondary loss results in a large percentage change due to small value of secondary loss and hence it is not possible to accurately estimate percentage reduction in secondary loss values for such cases. This suggests that the optimization objective should be total loss reduction and not the secondary loss reduction.
- Analysis indicates that end wall contouring results in a small performance gain on this design due to its low predicted level of secondary and end wall losses. It is expected that for the designs with low aspect ratios, increased airfoil loading, more front loaded blades etc., where secondary losses are a significant portion of total loss, end wall contouring may result in larger performance gains.
- Secondary losses are usually higher at off design conditions when there is a large positive incidence angle. Effect of end wall contouring at off-design performance should be investigated for such high exit Mach number blades to make an overall assessment of effect of end wall contouring.
- It seems that SKE is not the primary factor affecting the mass averaged total pressure losses. End wall contouring was found to reduce SKE to a near optimum value. Hence, a correct approach for end wall contouring optimization is reduction in mass averaged total pressure loss and not the reduction in SKE values. However, it may be possible to achieve better flow distribution in front of the blade by contouring both the end walls of vanes.
- Previous studies show that the CFD results frequently under predict the losses. Cascade testing of contoured end wall is planned to experimentally investigate the effectiveness of optimized contours in loss reduction.

REFERENCES

[1] Morris, A. W. H., Hoare, R. G., 1975, "Secondary loss measurements in a cascade of turbine blades with meridional wall profiling," ASME Paper 75-WA/GT-13.

[2] Kopper, F. C., Milano, R., 1981, "Experimental investigation of endwall profiling in a turbine vane cascade," AIAA Journal, Vol. 19(8), pp 1033-1040

[3] Duden, A., Raab, I., Fottner, L., 1998, "Controlling the secondary flow in a turbine cascade by 3D airfoil design and endwall contouring," International gas turbine & aeroengine conference & Exhibition, Stockholm, Sweden, 98-GT-72.

[4] Rose, M. G., 1994, "Non-axisymmetric endwall profiling in the HP NGV's of an axial flow gas turbine," International gas turbine and aeroengine congress and exposition, 94-GT-249.

[5] Harvey, N. W., Rose, M. G., Taylor, M. D., Shahpar, S., Hartland, J., Gregory-Smith, D. G., 2000, " Nonaxisymmetric turbine end wall design: Part I- three-dimensional linear design system," ASME Jl. of turbomachinery, Vol. 122, April 2000, pp278-285.

[6] Hartland, J. C., Gregory-Smith, D. G., Harvey, N. W., Rose, M. G., 2000, " Nonaxisymmetric turbine end wall design: Part II – Experimental validation," ASME Jl. of turbomachinery, Vol. 122, April 2000, pp286-293.

[7] Hartland, J., Gregory-Smith, D. G., 2002, "A design method for the profiling of end walls in turbines", Proceedings of ASME turboexpo 2002, June 3-6, Amsterdam, The Netherlands, GT-2002-30433.

[8] Nagel, M. G., Baier, R. D., 2005, "Experimentally verified numerical optimization of a three-dimensional parameterized turbine vane with nonaxisymmetric end walls," ASME Jl. of turbomachinery, Vol. 127, April 2005, pp380-387.

[9] Saha, A. K., Acharya, S., 2006, "Computations of turbulent flow and heat transfer through a three-dimensional non-axisymmetric blade passage," Proceedings of GT2006, ASME Turbo Expo 2006: power for land, sea and air, May 8-11, Barcelona, Spain, GT2006-90390.

[10] Gustafson, R., Mahmood, G., Acharya, S., 2007, "Aerodynamic measurements in a linear turbine blade passage with three-dimensional endwall contouring," Proceedings of GT2007, ASME Turbo Expo 2007: power for land, sea and air, May 14-17, Montreal, Canada, GT2007-28073.

[11] Praisner, T. J., Allen-Bradley, E., Grover, E. A., Knezevici, D. C., Sjolander, S. A., 2007, "Application of non-axisymmetric endwall contouring to conventional and high-lift turbine airfoils," Proceedings of GT2007, ASME Turbo Expo 2007: power for land, sea and air, May 14-17, Montreal, Canada, GT2007-27579.

[12] Snedden, G., Dunn D., Ingram, G., Gregory-Smith D., 2009, "The application of non-axisymmetric endwall contouring in a single stage, rotating turbine," Proceedings of GT2009, ASME Turbo Expo 2009: Power for land, sea and air, June 8-12, Orlando, Florida, GT2009-59169.

[13] Piegl, L. A., Tiller, W., 1996, The NURBS book (Monographs in visual communication), Springer, 2nd edition, New York, Chap. 9.

[14] Oberkampf, W. L., Roy, C., J., 2010, Verification and validation in scientific computing, Cambridge university press, 1st ed., New York.

[15] Schittkowski, K., 1985, NLPQL: A FORTRAN subroutine solving constrained nonlinear optimization problems, Annals of operations research 5 ,1985/6, pp485-500.